Stem Cell Reports
Article
ISSCR
OPEN ACCESS

Parallel use of human stem cell lung and heart models provide insights for SARS-CoV-2 treatment

Rajeev Rudraraju,[1,15] Matthew J. Gartner,[1,15] Jessica A. Neil,[1,15] Elizabeth S. Stout,[2,15] Joseph Chen,[3,4,5,15] Elise J. Needham,[6,15] Michael See,[2,7,15] Charley Mackenzie-Kludas,[1] Leo Yi Yang Lee,[1] Mingyang Wang,[1] Hayley Pointer,[2] Kathy Karavendzas,[2] Dad Abu-Bonsrah,[2] Damien Drew,[8] Yu Bo Yang Sun,[3,4,5] Jia Ping Tan,[3,4,5] Guizhi Sun,[3,4,5] Abbas Salavaty,[5,9] Natalie Charitakis,[2,13] Hieu T. Nim,[2,5,13] Peter D. Currie,[5,9] Wai-Hong Tham,[8,10] Enzo Porrello,[2,11,12,16,*] Jose M. Polo,[3,4,5,16,*] Sean J. Humphrey,[6,16,*] Mirana Ramialison,[2,5,13,16,*] David A. Elliott,[2,5,13,16,*] and Kanta Subbarao[1,14,16,*]

[1]The Department of Microbiology and Immunology, The Peter Doherty Institute for Infection and Immunity, The University of Melbourne, Melbourne, VIC, Australia
[2]The Novo Nordisk Foundation Centre for Stem Cell Medicine (reNEW), Murdoch Children's Research Institute, Melbourne, VIC, Australia
[3]Department of Anatomy and Developmental Biology, Monash University, Clayton, VIC, Australia
[4]Development and Stem Cells Program, Monash Biomedicine Discovery Institute, Clayton, VIC, Australia
[5]Australian Regenerative Medicine Institute, Monash University, Clayton, VIC, Australia
[6]Charles Perkins Centre and School of Life and Environmental Sciences, Faculty of Science, The University of Sydney, Camperdown, NSW, Australia
[7]Monash Bioinformatics Platform, Monash University, Clayton, VIC, Australia
[8]Infection and Immunity Division, The Walter and Eliza Hall Institute of Medical Research, Parkville, VIC, Australia
[9]EMBL Australia, Monash University, Clayton, VIC, Australia
[10]Department of Medical Biology, The University of Melbourne, Melbourne, VIC, Australia
[11]Melbourne Centre for Cardiovascular Genomics and Regenerative Medicine, The Royal Children's Hospital, Melbourne, VIC, Australia
[12]Department of Anatomy and Physiology, School of Biomedical Sciences, The University of Melbourne, Parkville, VIC, Australia
[13]Department of Pediatrics, The Royal Children's Hospital, University of Melbourne Parkville, VIC, Australia
[14]The WHO Collaborating Centre for Reference and Research on Influenza, The Peter Doherty Institute for Infection and Immunity, Melbourne, VIC, Australia
[15]These authors contributed equally
[16]Senior and corresponding author
*Correspondence: enzo.porrello@mcri.edu.au (E.P.), jose.polo@monash.edu (J.M.P.), sean.humphrey@mcri.edu.au (S.J.H.), mirana.ramialison@mcri.edu.au (M.R.), david.elliott@mcri.edu.au (D.A.E.), kanta.subbarao@influenzacentre.org (K.S.)
https://doi.org/10.1016/j.stemcr.2023.05.007

SUMMARY

Severe acute respiratory syndrome coronavirus 2 (SARS-CoV-2) primarily infects the respiratory tract, but pulmonary and cardiac complications occur in severe coronavirus disease 2019 (COVID-19). To elucidate molecular mechanisms in the lung and heart, we conducted paired experiments in human stem cell-derived lung alveolar type II (AT2) epithelial cell and cardiac cultures infected with SARS-CoV-2. With CRISPR-Cas9-mediated knockout of *ACE2*, we demonstrated that angiotensin-converting enzyme 2 (ACE2) was essential for SARS-CoV-2 infection of both cell types but that further processing in lung cells required TMPRSS2, while cardiac cells required the endosomal pathway. Host responses were significantly different; transcriptome profiling and phosphoproteomics responses depended strongly on the cell type. We identified several antiviral compounds with distinct antiviral and toxicity profiles in lung AT2 and cardiac cells, highlighting the importance of using several relevant cell types for evaluation of antiviral drugs. Our data provide new insights into rational drug combinations for effective treatment of a virus that affects multiple organ systems.

INTRODUCTION

Coronavirus disease 2019 (COVID-19) is primarily a respiratory disease, with 80% of infections clinically mild or asymptomatic. Progression to severe illness is associated with lower respiratory tract involvement (Chen et al., 2021b; Hou et al., 2020). In addition to pulmonary disease, cardiovascular, renal, digestive, and neurological complications are reported (Nalbandian et al., 2021). Cardiac complications include arrhythmias, thromboembolism, and acute myocardial injury (Lazzerini et al., 2022; Shi et al., 2020). Cardiac involvement is observed in up to 78% of recovered COVID-19 patients, and ongoing myocardial inflammation is observed in 60% of patients (Goyal et al., 2020; Puntmann et al., 2020). Furthermore, myocardial injury was associated with increased mortality (Shao et al., 2020). While cardiac damage during COVID-19 is predominantly thought to be due to an over-exuberant immune response, studies of autopsy tissue from patients who died from COVID-19 have detected viral RNA and spike (S) antigen in the heart (Deinhardt-Emmer et al., 2021; Schneider et al., 2020; Wang et al., 2021).

Severe acute respiratory syndrome coronavirus 2 (SARS-CoV-2) mediates infection by binding of the S protein to its receptor, angiotensin-converting enzyme 2 (ACE2) (Zhou et al., 2020). The S protein is cleaved into two domains, S1 and S2, by host cell proteases (Shang et al., 2020). Following attachment, fusion with the cell

membrane requires further proteolytic cleavage at the S2′ site to activate the fusion peptide (Hoffmann et al., 2020). This is mediated extracellularly by serine proteases including transmembrane protease, serine 2 (TMPRSS2) or in endosomes by cathepsin L (Hoffmann et al., 2020; Ou et al., 2020; Perez-Bermejo et al., 2021). Thus, ACE2 is a critical determinant of the tissue tropism of SARS-CoV-2, as is the presence of surface and/or endosomal proteases. ACE2 is expressed in many human tissues, with the highest ACE2 expression observed in the nasal epithelium, lungs, ileum, and heart (Hamming et al., 2004; Muus et al., 2021; Qi et al., 2020; Sungnak et al., 2020; Zou et al., 2020). Tissue sites containing cells that co-express ACE2 and TMPRSS2 include the nose, lungs, kidney, gastrointestinal tract, and the gallbladder (Muus et al., 2021; Sungnak et al., 2020), while cells co-expressing ACE2 and cathepsin L are found within the lung, heart, and gastrointestinal tract (Muus et al., 2021). Following entry, the virus interacts with cellular machinery to complete its replication cycle and triggers a host cell response that can vary in different organs.

We sought to elucidate the molecular mechanisms of SARS-CoV-2 infection in lung and heart using human stem cell-derived lung and cardiac cells. Human pluripotent stem cells (hPSCs) including both human embryonic stem cells (hESCs) and induced pluripotent stem cells (hiPSCs) have been used to generate functional human cells, tissues, and organoids to model human disease. We and others have generated stem cell-derived lung alveolar type II (AT2) epithelial cell and cardiac cultures that can be productively infected with SARS-CoV-2 (Huang et al., 2020; Perez-Bermejo et al., 2021; Sharma et al., 2020; Williams et al., 2021). We hypothesized that paired experiments in SARS-CoV-2-infected lung and cardiac cells would reveal important similarities and differences in viral and host factors that could inform treatment of COVID-19 and its complications. We used CRISPR-Cas9-mediated knockout of ACE2 and demonstrated that ACE2 was essential for SARS-CoV-2 infection of both cell types. Small-molecule inhibitors revealed distinct mechanisms of SARS-CoV-2 entry. We identified differential cellular responses to SARS-CoV-2 infection by transcriptome profiling and phosphoproteomics and further demonstrated the utility of these stem cell-derived models for screening antiviral compounds for anti-SARS-CoV-2 activity. Our findings provide new insights into treatment strategies for COVID-19.

RESULTS

SARS-CoV-2 productively infects human stem cell-derived lung AT2 and cardiac cultures

hESC- and iPSC-derived cardiomyocyte (Anderson et al., 2018; Lopes et al., 2021) and AT2 lung (Jacob et al., 2017) cultures were generated to develop *in vitro* models of SARS-CoV-2 infection (Figure 1A). Lung AT2 cultures expressed the AT2 cellular markers surfactant protein C (SFTPC) and HT2-280, along with the lung development homeobox protein NKX2-1 and an absence of aquaporin-5 (AQP5), FOXJ1, and SCGB3A2, confirming differentiation into AT2 cells (Figure S1A). Gene expression profiling of the lung AT2 and cardiac cells demonstrated transcriptional profiles consistent with high levels of AT2 cells and cardiomyocytes, respectively (Figures S1B and S1C).

To determine susceptibility to SARS-CoV-2 infection, lung AT2, cardiac, and Vero cells were inoculated with the ancestral strain of SARS-CoV-2. As expected, SARS-CoV-2 productively infected Vero cells with virus titers and E gene copies peaking at 3 days post-infection (dpi) (Figure 1B). SARS-CoV-2 showed robust virus replication in AT2 cells, with virus titers and E gene copies peaking at 4 dpi (Figure 1B). Immunostaining for double-stranded RNA (dsRNA) showed evidence of SARS-CoV-2 replication at 3 dpi (Figure 1C). Cardiac cell cultures differentiated from hESCs (*NKX2-5*$^{eGPF/w}$ [Elliott et al., 2011]) were also susceptible to SARS-CoV-2 infection, with virus titers and E gene copies peaking slightly later than AT2 cells between 4 and 6 dpi (Figure 1B). Cardiac cells generated from *ALPK3* knockout hESCs that model hypertrophic cardiomyopathy (Phelan et al., 2016), were similarly susceptible to SARS-CoV-2 infection, with a peak in virus titers at 4 dpi (Figure S1D). Immunostaining showed SARS-CoV-2 dsRNA in both cardiomyocyte and non-cardiomyocyte cells within the cardiac cultures (Figure 1C). Furthermore, cardiac cultures infected with SARS-CoV-2 stopped contracting at 4 dpi (Video S1). Overall, these data show that SARS-CoV-2 replicates efficiently in cardiac and lung AT2 cells, consistent with published reports (Huang et al., 2020; Perez-Bermejo et al., 2021).

To determine susceptibility to SARS-CoV-2 variants, cardiac and AT2 cells were inoculated with Alpha, Beta, Gamma, Delta, and Omicron (BA.1 and BA.2) variants. Although all variants were able to infect AT2 cells, a modest difference was observed following Delta infection at 1 and 3 dpi (Figures 1D and S1E), with titers comparable to all other variants by 5 dpi. In cardiac cells, a slightly lower virus titer was observed following infection with the Alpha variant at 3 dpi (Figure 1D). However, this was not observed for E gene copies where wild-type (WT) levels were higher than other variants on 1 and 3 dpi (Figure S1E). In AT2 cells, the Omicron subvariants showed similar titers to the WT virus, although BA.1 showed a modest reduction in virus titers and E gene copies compared with BA.2 (Figures 1E and S1F). In cardiac cells, the BA.1 and BA.2 variants showed lower virus titers compared with the WT virus at 2–5 dpi

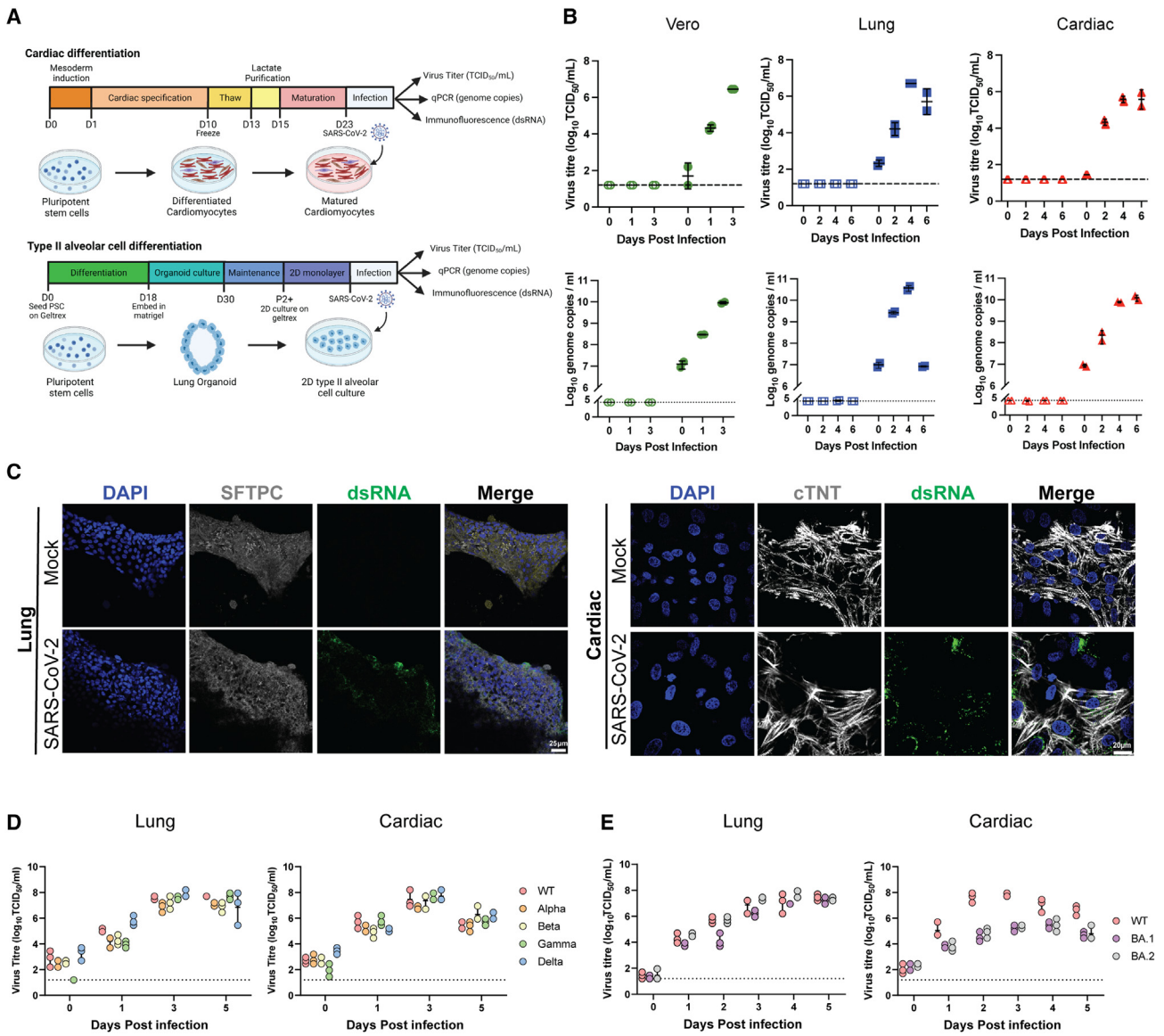

Figure 1. SARS-CoV-2 infection of cardiac and lung AT2 cells

(A) Schematic of cell differentiation and infection protocols.

(B) Viral titers and genome copies in SARS-CoV-2 (VIC01)-infected Vero, lung AT2 (H9), and cardiac (NKX2-5) culture supernatants. Data are presented as mean ± SD. Results are representative of two independent experiments each with 2 technical replicates.

(C) Representative fluorescent confocal microscopy images of dsRNA (green) expression in infected lung AT2 (SFTPC-positive) and cardiac (cTNT-positive) cells at 3 dpi.

(D and E) Titers in supernatants from cardiac (NKX2-5) and lung AT2 cells infected with VIC01 (WT) compared with cells infected with Alpha, Beta, Gamma, and Delta variants (D) or Omicron (BA.1 and BA.2) variants (E). Data are presented as mean ± SD. Results are representative of two independent experiments each with 3 technical replicates.

See also Figure S1.

(Figure 1E). However, this difference in replication was not observed for E gene copies (Figure S1F). These data confirm that hPSC-derived *in vitro* models can be used to study SARS-CoV-2 and that SARS-CoV-2 variants infect cardiac and lung cells efficiently.

SARS-CoV-2 infection in lung AT2 and cardiac cells is dependent on ACE2

To confirm that ACE2 is required for SARS-CoV-2 infection in cardiac and lung AT2 cells, we generated two *ACE2* knockout (KO) hPSC lines (H9 and MCRIi010-A; Figure S2A

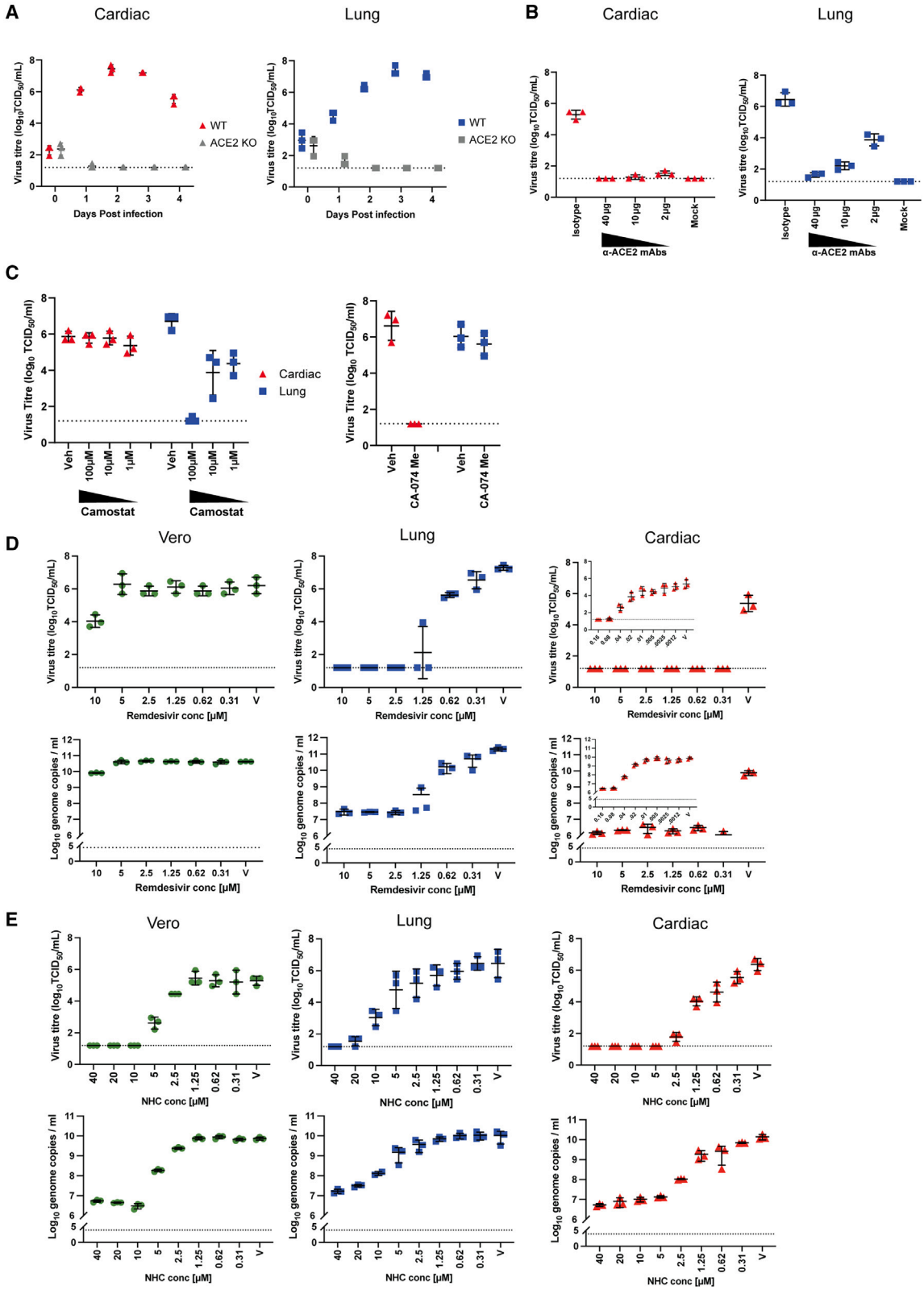

(legend on next page)

and S2B). ACE2 protein and *ACE2* transcript expression was not detected in either AT2 or cardiac cultures differentiated from the *ACE2* KO line (Figures S2C, S2D, and S2I). Flow cytometric analysis confirmed that the genetically modified cells maintained their expression of pluripotency markers and showed similar differentiation capacity (Figures S2E–S2G). The *ACE2* KO cardiac or AT2 cells could not be productively infected with SARS-CoV-2 as shown by the inability to recover infectious virus and absence of dsRNA staining (Figures 2A, S2H, and S2I). For independent confirmation of the role of ACE2, we used a combination of two previously described α-ACE2 antibodies (Chen et al., 2021a). In cardiac cultures, 2 μg/mL α-ACE2 antibodies was sufficient to completely block SARS-CoV-2 infection (Figure 2B). In contrast, treatment with the α-ACE2 antibody cocktail blocked infection in a dose-dependent fashion in AT2 cells (Figure 2B). Overall, our data demonstrate that SARS-CoV-2 infection in lung AT2 and cardiac cells is ACE2 dependent.

SARS-CoV-2 utilizes differential entry mechanisms in lung AT2 and cardiac cells

To determine the mechanism of entry, cells were infected in the presence of the TMPRSS2 inhibitor camostat mesylate or the cathepsin B/L inhibitor CA-074 Me. Camostat treatment led to a dose-dependent reduction in virus titer and genome copies in AT2 but not in cardiac cells (Figures 2C and S3C), showing that infection in lung AT2 cells requires TMPRSS2 cleavage. In contrast, CA-074 Me led to a complete inhibition of virus replication in cardiac but not in AT2 cells (Figures 2C and S3C), confirming that viral entry in cardiac cells requires the endosomal pathway. This is consistent with the high expression of *TMPRSS2* observed in lung AT2 cells and the absence of *TMPRSS2* in cardiac cells (Figures S3A and S3B). Although expression of TMPRSS2 by cardiomyocytes has been observed by two studies (Lee et al., 2021; Williams et al., 2021), the majority suggest that TMRPSS2 expression is low or absent in these cells (Navaratnarajah et al., 2021; Perez-Bermejo et al., 2021; Robinson et al., 2020; Yang et al., 2021). Thus, consistent with the gene expression data, SARS-CoV-2 utilizes distinct entry pathways in lung AT2 and cardiac cells.

Antiviral compounds show differential activity in lung and cardiac cells compared with traditional cell lines

To determine whether SARS-CoV-2 antiviral drugs show similar activity in lung AT2 and cardiac cells, we investigated two sets of small molecules: (1) drugs that are approved for treatment of COVID-19 including remdesivir and NHC (β-D-N4-hydroxycytidine), the prodrug of molnupiravir, and (2) drugs that were reported to show antiviral activity *in vitro* but are still under clinical investigation or were not found to be effective in clinical trials including favipiravir, tizoxanide (the active form of the antiparasitic agent nitazoxanide), and chloroquine.

In Vero cells, remdesivir inhibited virus replication at a concentration of 10 μM, while in lung AT2 cells and cardiac cells, the drug completely inhibited virus replication at 2.5 and 0.08 μM, respectively (Figure 2D). NHC was also more effective in inhibiting virus replication in cardiac cells compared with AT2 and Vero cells, with complete virus inhibition observed at 5 μM, while viral replication was inhibited in Vero and AT2 cells with similar dose-response kinetics (Figure 2E). Toxicity of remdesivir and NHC in AT2 and cardiac cells was observed with concentrations above 5 and 40 μM, respectively (Figures S3D and S3E). Favipiravir, piperaquine, and tizoxanide showed no antiviral activity against SARS-CoV-2 in cardiac, AT2, and Vero cells up to a concentration of 10 μM (Figure S3F). Chloroquine inhibited SARS-CoV-2 virus replication in cardiac cells (including the *ALPK3* KO cardiomyopathy model) but not in AT2 or Vero cells (Figure S3F), consistent with our observation that SARS-CoV-2 entry in cardiac cells utilizes the endosomal pathway. These results highlight the variability in antiviral efficacy in different cell types and emphasize the relevance of using hPSC-derived models over Vero cells for assessment of antiviral drugs for COVID-19.

SARS-CoV-2 induces different transcriptional responses in lung AT2 and cardiac cells

Based on our observation of distinct entry pathways and antiviral activity between lung AT2 and cardiac cells, we hypothesized that they would show diverse responses to

Figure 2. SARS-CoV-2 infection is ACE2 dependent but further steps in entry and antiviral sensitivity are different between lung AT2 and cardiac cells

(A) Virus titer in supernatants from SARS-CoV-2 (VIC01)-infected H9-derived WT and *ACE2* KO cardiac and lung AT2 cells.

(B) Virus titer at 3 dpi in supernatants from lung AT2 (H9) and cardiac cells (NKX2-5) treated with two α-ACE2 antibodies or a human IgG1 isotype control before infection with SARS-CoV-2.

(C) Virus titer at 3 dpi in supernatant from cardiac cells (NKX2-5, red triangles) and lung AT2 cells (blue squares) infected with SARS-CoV-2 (VIC01) in the presence of camostat, CA-074 Me, or DMSO (vehicle control).

(D and E) Virus titers and genome copies at 3 dpi in supernatant from Vero, lung AT2, and cardiac cells (NKX2-5) infected with SARS-CoV-2 VIC01 in the presence of various concentrations of Remdesivir (D) or NHC (E). Data are presented as mean ± SD. Results are representative of two independent experiments each with 3 technical replicates.

See also Figure S2 and S3.

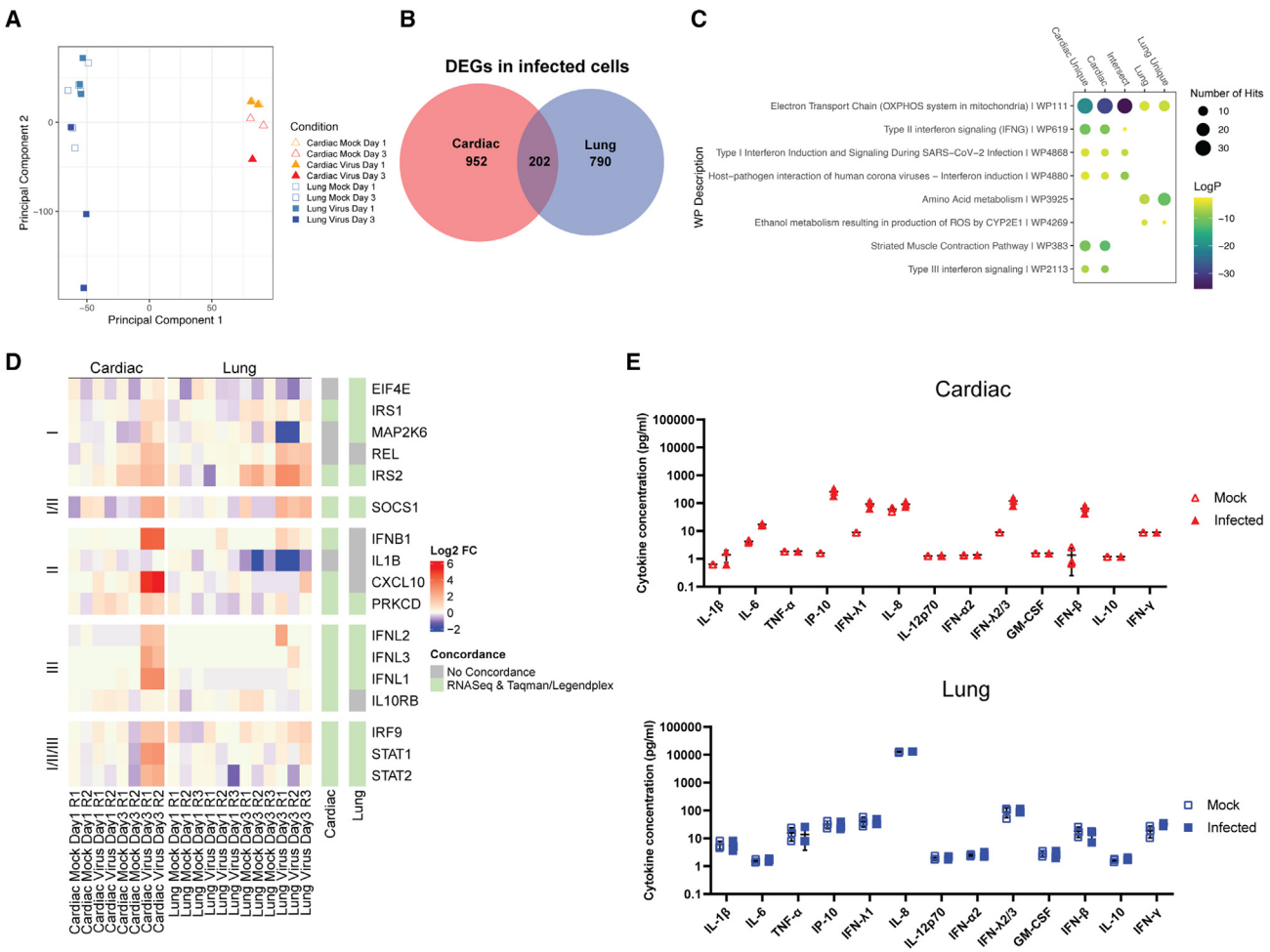

Figure 3. Cardiac cells have a stronger interferon signature than lung AT2 cells following SARS-CoV-2 infection

(A) Principal-component analysis (PCA) plot of uninfected (mock) and SARS-CoV-2-infected (virus) cardiac (H9) and lung AT2 cells at 1 and 3 dpi.

(B) Venn diagram depicting the number of overlapping and unique differentially expressed genes compared with mock.

(C) Extended plot of top enriched WP terms from total cardiac, total lung, intersect, lung unique, and cardiac unique differentially expressed genes. Circle size is proportional to the number of genes that matched the pathway, and color represents the logp value as calculated by Metascape.

(D) Heatmap in log2 fold change (FC) of representative interferon genes (compared with representative mock samples at 1 dpi) separated by type as defined by WikiPathways. Columns on the right show the concordance between direction of FC of RNA-seq data and the LegendPlex/Taqman assays. For 1 and 3 dpi, 3 lung samples and 2 cardiac samples were analyzed per group (mock, virus).

(E) Cytokine concentrations in supernatants of mock- and SARS-CoV-2-infected cardiac and lung AT2 cells at 3 dpi. Data are presented as mean ± SD. Results are representative of two independent experiments each with 3 technical replicates. See also Figure S4.

SARS-CoV-2 infection. RNA sequencing (RNA-seq) was performed on cell lysates from lung AT2 and cardiac cells infected with SARS-CoV-2 at 1 and 3 dpi. Principal-component analysis (PCA) separated the tissue types and demonstrated a progressive separation between mock and infected cells (Figure 3A). At 1 dpi, no differentially expressed genes (DEGs) were observed in AT2 cells, and only 5 were observed in cardiac cells (data not shown). However, at 3 dpi, 1,154 and 992 DEGs were obtained for cardiac and AT2 cells, respectively. As shown in Figure 3B, of the DEGs between the two cell types, 202 were overlapping ("intersect"), 952 genes were differentially expressed in the cardiac cells only ("cardiac unique"), and 790 genes were differentially expressed in the lung AT2 cells only ("lung unique"). Additionally, we found that SARS-CoV-2 infection did not change the expression profile of lung development genes in AT2 cells and cardiac development genes in cardiac cells at 1 and 3 dpi (Figures S1B and S1C).

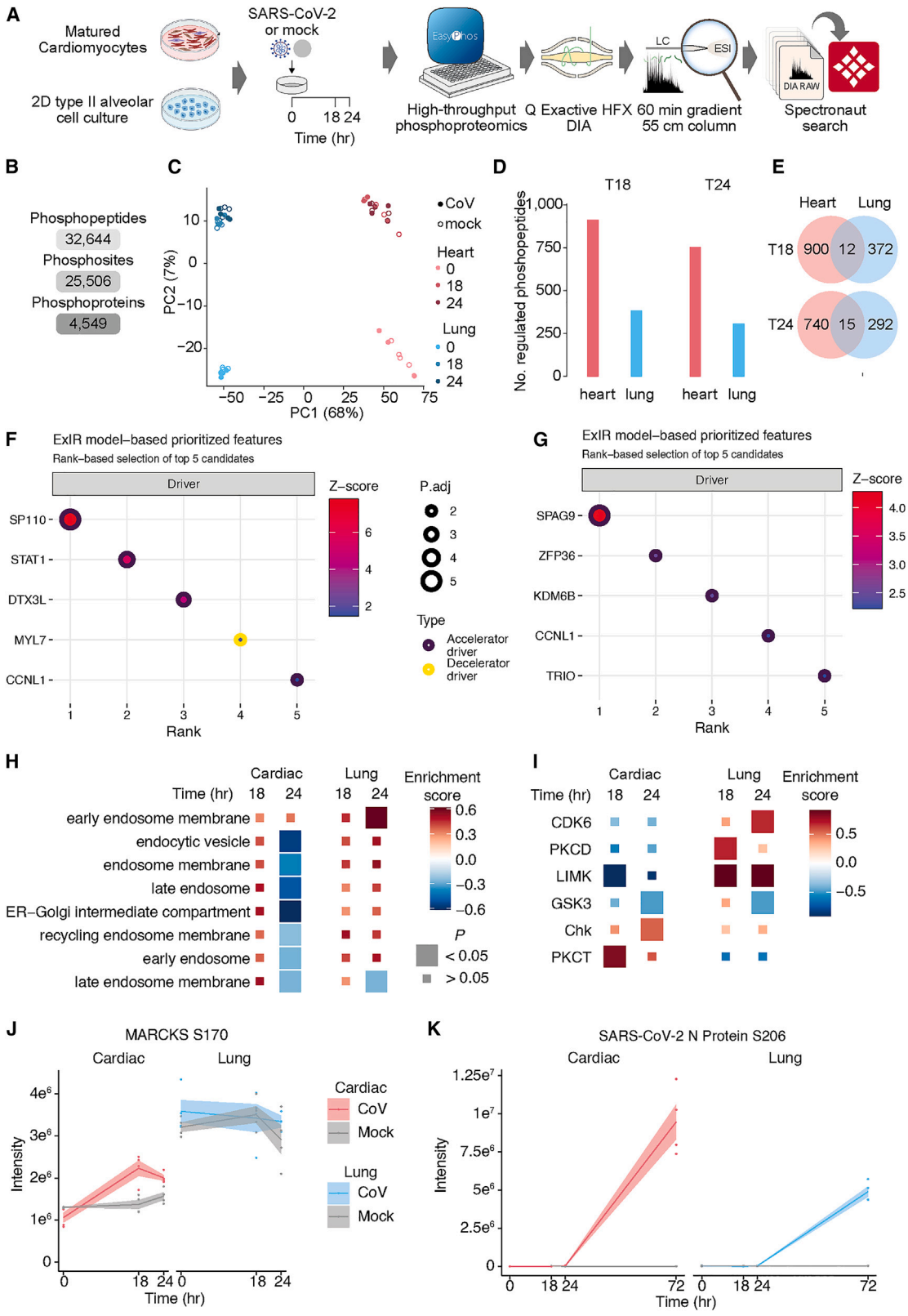
A
Matured Cardiomyocytes
2D type II alveolar cell culture
SARS-CoV-2 or mock
0 18 24
Time (hr)
High-throughput phosphoproteomics
Q Exactive HFX DIA
LC
ESI
60 min gradient 55 cm column
DIA RAW
Spectronaut search
B
Phosphopeptides
32,644
Phosphosites
25,506
Phosphoproteins
4,549
C
PC2 (7%)
PC1 (68%)
CoV
mock
Heart
0
18
24
Lung
0
18
24
D
T18
T24
No. regulated phoshopeptides
heart lung heart lung
E
Heart Lung
T18 900 12 372
T24 740 15 292
F
ExIR model–based prioritized features
Rank–based selection of top 5 candidates
Driver
SP110
STAT1
DTX3L
MYL7
CCNL1
Rank
Z–score
P.adj
Type
Accelerator driver
Decelerator driver
G
ExIR model–based prioritized features
Rank–based selection of top 5 candidates
Driver
SPAG9
ZFP36
KDM6B
CCNL1
TRIO
Rank
Z–score
H
Cardiac
Lung
Time (hr) 18 24
early endosome membrane
endocytic vesicle
endosome membrane
late endosome
ER–Golgi intermediate compartment
recycling endosome membrane
early endosome
late endosome membrane
Enrichment score
P
< 0.05
> 0.05
I
Cardiac
Lung
Time (hr) 18 24
CDK6
PKCD
LIMK
GSK3
Chk
PKCT
Enrichment score
J
MARCKS S170
Cardiac
Lung
Intensity
Time (hr)
Cardiac
CoV
Mock
Lung
CoV
Mock
K
SARS-CoV-2 N Protein S206
Cardiac
Lung
Intensity
Time (hr)

WikiPathway (WP) enrichment analysis of DEG subsets identified that the biological processes impacted by SARS-CoV-2 infection in both lung AT2 and cardiac cells (intersect subset) included genes involved in cellular processes including the electron transport chain (WP111) and oxidative phosphorylation (WP623) and genes involved in interferon (IFN) signaling (WP4880, WP4868, and WP619; Figures 3C, S4A, and S4B). We also found DEGs in both AT2 and cardiac cells associated with cell death or apoptosis (WP254 and WP615). In cardiac cells, we found an upregulation of genes in type III IFN signaling (WP2113) and a downregulation of genes associated with striated muscle contraction (WP383), consistent with the cessation of contractility of SARS-CoV-2-infected cultures (Video S1). In lung AT2 cells, we observed an overall downregulation of genes in amino acid metabolism (WP3925) and an upregulation of genes associated with production of reactive oxygen species (WP4269) (Figure 3C).

Key differences in the transcriptional responses to SARS-CoV-2 infection between AT2 and cardiac cells were the IFN pathways that were activated (Figures 3C and 3D). While IFN signaling was overall activated in both systems (Figure 3C, intersect), we observed differences in activation in specific IFN pathway components. By 3 dpi, genes from the type I, II, and III IFN pathways (*IFNB1*, *CXCL10*, *PRKCD*, *IFNL1*, *IFNL2*, and *IFNL3*) were strongly upregulated in cardiac compared with lung AT2 cells showing weaker changes (Figure 3D). Concordant with the observed increase in transcription by RNA-seq, cytokine analysis showed an induction of interleukin-6 (IL-6), IP-10, IFN-λ1, IFN-λ2/3, and IFN-β in infected cardiac cells, but not AT2 cells, at 3 dpi compared with mock controls (Figure 3E). Furthermore, qPCR showed induction of *IFITM3*, *IFN-β*, *STAT1*, and *STAT2* in infected cardiac cells, but not AT2 cells, compared with mock at 3 dpi (Figure S4C). Network analysis of the GO term response to IFN-γ showed that multiple genes within the network were upregulated in infected cardiac but not AT2 cells (Figure S4D). Taken together, SARS-CoV-2 infection induces IFN response in both cell types, but direct comparison of the pathway components indicates robust type I, II, and III IFN responses that are specific to cardiac cells only.

SARS-CoV-2 activates druggable kinases in lung AT2 and cardiac cells

We measured the phosphoproteome to determine the signaling responses of lung AT2 and cardiac cells to SARS-CoV-2 infection at 0, 18, 24, and 72 h post-inoculation (Figure 4A). Viral phosphorylation sites were analyzed at 72 h only. By employing recent advances in phosphoproteomics technologies (Humphrey et al., 2018), we quantified >32,000 phosphopeptides in at least three samples (Figure 4B). The phosphoproteomes clustered primarily by tissue origin in PCA (PC1), emphasizing the cell-type-specific nature of signaling (Figure 4C). Time since infection was the second largest factor affecting clustering by PCA (on PC2) due to the long time points studied. For this reason, a mock condition was sampled at every time point, enabling identification of infection-driven signaling. SARS-CoV-2 infection extensively regulated cellular signaling, with at least 250 phosphopeptides regulated at each time point (Figure 4D). Regulation of the phosphoproteome was most extensive in cardiac cells at 18 h post-infection (>900 phosphopeptides altered). Remarkably, only 12 and 15 phosphopeptides were commonly regulated between the cardiac and lung AT2 cells at the 18 and 24 h time points, respectively (Figure 4E). This low overlap of regulation was also observed at the transcriptional level and indicates that the response to SARS-CoV-2 is highly contextual and depends strongly on the cell type or tissue of origin.

To corroborate this, we sought to identify the molecular drivers of the SARS-CoV-2 infection response by integrating RNA-seq and phosphoproteomics datasets. The top 3 drivers of SARS-CoV-2 infection response in cardiac cells (*SP110*, *STAT1*, and *DTX3L*) were activators of the

Figure 4. SARS-CoV-2 infection alters different signaling networks in heart and lung organoids

(A) Schematic of phosphoproteomics workflow.

(B) Number of phosphorylated peptides, sites, and proteins found in 3 samples.

(C) PCA plot of median-normalized phosphoproteome replicates from uninfected (mock) and SARS-CoV-2-infected (CoV) cardiac (H9) and lung AT2 cells at 18 and 24 h post-infection.

(D and E) Number of significantly (adjusted p [padj] < 0.05, FC > 1.5) regulated phosphopeptides per timepoint (D) and their overlap (E) between cell types.

(F and G) Top 5 predicted drivers following SARS-CoV-2 infection in cardiac cells (F) and in lung cells (G) at 72 h post-infection. padj are calculated based on the computation of *Z* score probability distributions of a molecule to be a driver and adjusted using the Benjamini and Hochberg algorithm.

(H) GO cellular components enriched in at least one condition (p < 0.05) that are related to endosomes.

(I) Kinases with enriched substrates, which were selected for targeting.

(J) Abundance of the PKC substrate MARCKS S170.

(K) Abundance of the SRPK1 substrate SARS-CoV-2 nucleocapsid protein S206.

See also Figure S4.

IFN response (Figures 4F and 4G). In contrast, no strong IFN pathway activators were identified in the top drivers of the infection response in AT2 cells, confirming the robust IFN response seen in cardiac cells compared with AT2 cells. Endosomal components almost uniquely enriched in the SARS-CoV-2 response of cardiac cells but not AT2 cells (Figures 4H and S4E). This mirrors the pattern of viral entry occurring via endocytosis in cardiac cells.

By mapping reported kinase-substrate relationships to our phosphoproteomics data, we found that 37 kinases had substrates that were enriched for regulated phosphosites (Figures 4I and S4F). We hypothesized that kinases with substrates enriched in upregulated phosphorylation sites had increased activity in the SARS-CoV-2 response, and vice versa for kinases with downregulated sites. The unique signaling responses of cardiac and lung cells was also evident at the kinase level as, of the 37 kinases enriched in at least one condition, 6 were significantly enriched in the same direction in both cell types. For kinases such as protein kinase C (PKC), some isoforms had opposite cell-type-specific patterns of regulation. Of the PKC isoforms, PKCD had substrates enriched in upregulated sites in the lung AT2 cells, while PKCT was enriched in the cardiac cells (Figure 4I). This could suggest some convergence in signaling outcomes despite differing proteins being employed. However, the gold-standard PKC substrate MARCKS S170 was uniquely upregulated in cardiac cells (Figure 4J).

Since SARS-CoV-2 proteins can also be phosphorylated by host kinases, we also searched our phosphoproteomics data specifically for phosphorylation of SARS-CoV-2 viral proteins. We measured 32 sites on 5 viral proteins (ORF1a, S, M, N, and ORF9b; Table S1). This list includes S206 on the nucleocapsid protein, which has been reported as an SRSF protein kinase 1 (SRPK1) substrate (Figure 4K; Yaron et al., 2020).

Differential antiviral activity of candidate compounds in cardiac and lung AT2 cells

We interrogated our molecular datasets to predict new and alternative druggable targets. We selected 9 pathways that were differentially phosphorylated in SARS-CoV-2-infected lung AT2 and cardiac cells and identified 15 compounds that could inhibit the kinases critical for these pathways. These kinases (and their inhibitors) included: LIM domain kinase (R-10015); checkpoint kinases 2 (CCT241533 HCL); SRPK1 (Alectinib, SPHINX31); cyclin-dependent kinases (CDKs) (CCT251545, SNS-032, palbociclib hydrochloride, flavopiridol, dinaciclib, abemaciclib, samuraciclib hydrochloride hydrate, trilaciclib hydrochloride); glycogen synthase kinase-3 (AZD1080); and PKC (bisindolylmaleimide I). We also tested an inhibitor of the transforming growth factor β (TGF-β) pathway using an inhibitor of the TGF-β type II receptor (GW788388). We screened the compounds at 1, 10, and 50 μM for antiviral activity (data not shown), based on which we eliminated three compounds that targeted CDKs due to their strong toxicity in cardiac cells and lack of activity in lung cells (flavopiridol, dinaciclib, samuraciclib hydrochloride hydrate). SNS-032 was analyzed further although it was toxic in cardiac cells because it showed promising antiviral activity in AT2 cells. We evaluated the remaining 12 compounds across a dose range for antiviral activity and cell cytotoxicity in both cardiac (H9 and NKX2-5) and lung AT2 (H9) cells.

While the CDK8 inhibitor CCT251545 was ineffective in limiting SARS-CoV-2 replication (Figure S5), CDK4/6 inhibitors abemaciclib and palbociclib inhibited virus replication in both cell types, and CDK4/6 inhibitor trilaciclib hydrochloride inhibited it in cardiac cells with variable inhibition in the AT2 cells (Figure 5A). CDK2/7/9 inhibitor SNS-032 showed significant antiviral activity with minimal cytotoxicity in AT2 cells but was cytotoxic in cardiac cells (Figure 5A). In cardiac cells, but not AT2 cells, antiviral activity was also observed with the CHK and PKC inhibitors at concentrations that were not cytotoxic (Figures 5B and 5C).

Alectinib and SPHINX31, which inhibit SRPK1, inhibited viral replication in both AT2 and cardiac cells, with greater inhibition in AT2 cells (Figure 5D). Similar activity of these antiviral drugs was observed in H9-derived cardiac cells (Figure S5A). Drugs that targeted LIM domain kinase (R-10015) and TGF-β type II receptor (GW788388) showed no activity in either cell type (Figure S5B). The GSK-3 inhibitor AZD1080 showed no antiviral activity in H9-derived lung AT2 and cardiac cells (Figure S5). However, it did show antiviral activity in NKX2-5 cardiac cells against VIC01 but not the nLuc virus, suggesting that removal of ORF7a may affect drug sensitivity (Figure S5; Hou et al., 2020). Overall, these data show that inhibition of kinases with small molecular inhibitors can abrogate SARS-CoV-2 replication with differing effectiveness in cardiac and lung AT2 cells.

DISCUSSION

Our data from parallel evaluation of SARS-CoV-2 infection in stem cell-derived cardiac and lung AT2 cells provide valuable insights into virus-host interactions in tissues that are significantly affected in COVID-19, with implications for rational design of therapeutic interventions. We show that virus entry, cellular response, antiviral activity, and cytotoxicity differ in SARS-CoV-2-infected human cardiac and lung AT2 cells and antiviral activity in both human cell types differ from what is seen in African monkey kidney-derived Vero cells that are widely used for SARS-CoV-2 research. Virus entry in both human cell types is

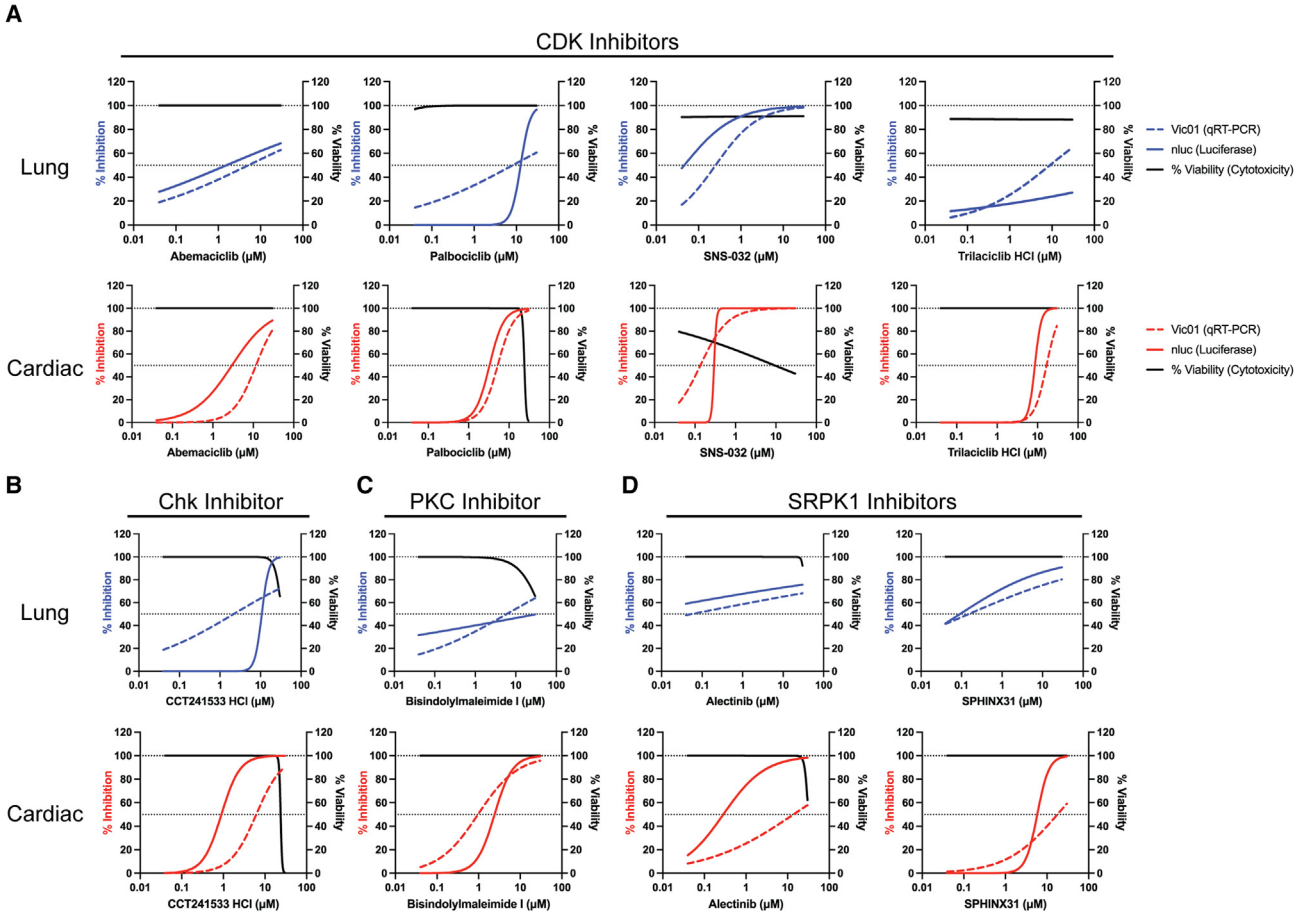

Figure 5. Efficacy of kinase inhibitors against SARS-CoV-2 replication varies between lung AT2 and cardiac cells

Cell viability (percentage relative to vehicle control, black lines) and inhibition of SARS-CoV-2 growth (percentage relative to vehicle control) in the presence of CDK (A), CHK (B), PKC (C), and SRPK1 (D) inhibitors in lung AT2 cells (H9) and cardiac cells (NKX2-5) at 2 dpi. Dotted black lines indicate 50% virus inhibition or cell viability. Results are representative of two independent experiments each with 3 technical replicates.

See also Figure S5.

dependent on ACE2, but further processing of the S protein is mediated through TMPRSS2 in lung AT2 cells, while infection of cardiac cells is achieved through the endosomal pathway and cathepsin L. Host responses are significantly different, with a robust IFN response signature specific in cardiac cells and a weaker response in lung AT2 cells. Phosphoproteomics analysis identified activation of different pathways in cardiac and lung AT2 cells. Parallel evaluation of antiviral activity and cytotoxicity of drugs in cardiac and lung AT2 cells reveals several points to consider in COVID-19 therapy, including the use of drug combinations to target both membrane protease and endosomal entry pathways, drugs that target SRPK1 and CDKs, and the importance of using relevant hPSC-derived models in place of immortalized cell lines such as Vero cells for assessment of antiviral drugs.

Early reports characterizing SARS-CoV-2 demonstrated the requirement of ACE2 for virus entry (Zhou et al., 2020). Similarly, we show that SARS-CoV-2 infection of *ACE2* KO lung AT2 and cardiac cells completely abolished virus growth, demonstrating that ACE2 is required for infection of these cells, consistent with previous reports using similar models (Bailey et al., 2021; Bojkova et al., 2020; Marchiano et al., 2021; Perez-Bermejo et al., 2021). Our RNA-seq and qPCR analyses of lung and cardiac cells demonstrated high ACE2 expression in lung AT2 cells and low expression in cardiac cells, despite robust viral growth. Anti-ACE2 antibodies at a low dose did not completely block infection in AT2 cells but did in cardiac cultures, likely reflecting this difference in ACE2 expression between the cell types. Overall, we show that ACE2 expression is required for

SARS-CoV-2 infection in hPSC-derived lung AT2 and cardiac cells.

To investigate the protease requirements for entry into hPSC-derived AT2 and cardiac cells, we performed entry inhibition assays with the TMPRSS2 inhibitor camostat mesylate and the cathepsin B/L inhibitor CA-074 Me (Montaser et al., 2002). Camostat inhibited SARS-CoV-2 infection in AT2 cells, suggesting that TMPRSS2 is required for SARS-CoV-2 infection of AT2 cells, consistent with previous reports (Huang et al., 2020; Tiwari et al., 2021). In contrast, CA-074 Me blocked SARS-CoV-2 infection in cardiac cells, demonstrating that cathepsin L cleavage through endosomal entry is required for infection of cardiac cells, consistent with previous studies (Bailey et al., 2021; Bojkova et al., 2020; Perez-Bermejo et al., 2021). The ability of SARS-CoV-2 to enter cells through different pathways may explain why clinical trials of camostat mesylate in hospitalized COVID-19 patients and hydroxychloroquine alone did not result in clinical benefit (Gunst et al., 2021). Our data suggest that a combination of drugs that target both pathways may be more effective *in vivo* and emphasize the importance of antiviral testing in several relevant tissue types.

We found a robust IFN response in cardiac cells. Induction of IFN in infected cardiac cell cultures has been previously reported using bulk RNA-seq (Bailey et al., 2021; Marchiano et al., 2021). However, Perez-Bermejo et al. reported that single-cell RNA-seq of infected iPSC-derived cardiomyocytes showed an induction of proinflammatory cytokines but not type I or III IFNs (Perez-Bermejo et al., 2021). A potential explanation for the discrepancy between our findings and those of Perez-Bermejo et al. is that the additional cells present in our cultures (fibroblasts, smooth muscle cells, and endothelial cells; Mills et al., 2017) or bystander cardiomyocytes are responsible for inducing robust IFN responses.

In contrast to cardiac cells, SARS-CoV-2 infection led to a weak IFN response in lung AT2 cells at 3 dpi. This is consistent with Li et al., who found a weak induction of IFN-β and IFN-λ at 2 dpi with SARS-CoV-2 in hPSC-derived AT2 cultures (Li et al., 2021). In contrast, Huang et al. found a moderate IFN response in hPSC-derived AT2 cells (Huang et al., 2020) and other studies using AT2 cells derived from primary cells found a stronger induction of the IFN response (Katsura et al., 2020; Mulay et al., 2021; Youk et al., 2020). This suggests that the level of IFN induction after SARS-CoV-2 infection of AT2 cells is dependent on the model system and virus dose.

The difference in host response to infection between cardiac cells and lung AT2 cells in our study may be explained by the viral entry pathways. SARS-CoV-2 replication leads to detection of dsRNA replication intermediates by melanoma-differentiation-associated gene 5 (MDA5) and induction of a robust IFN response through mitochondrial antiviral signaling protein (MAVS) signaling (Li et al., 2021; Sampaio et al., 2021). Several studies have identified SARS-CoV-2 proteins (nsp1, nsp5, nsp6, nsp13, nsp15, ORF6, and ORF7b) that inhibit MAVS-induced type I and III IFN responses (Lei et al., 2020; Shemesh et al., 2021; Xia et al., 2020). This mechanism of IFN antagonism likely explains the lack of IFN induction seen in lung AT2 cells following SARS-CoV-2 infection. In contrast, endosomal entry of SARS-CoV-2 in cardiac cells may explain the robust induction of IFN. Endosomes contain Toll-like receptors (TLRs) including TLR3 and TLR7/8 that sense dsRNA and single-stranded RNA (ssRNA), with only TLR3 detectable in cardiomyocytes (Uhlen et al., 2015). Furthermore, defects in TLR3 have been associated with disease severity in patients (Zhang et al., 2020), suggesting that TLR3 may play an important role in inducing IFN responses.

Although COVID-19 vaccines are highly effective in preventing severe illness and death, antiviral compounds are required for the treatment of COVID-19, particularly with the emergence of variant viruses and reduced effectiveness of vaccines in preventing symptomatic illness caused by variants of concern. To date, only a handful of drugs including remdesivir, molnupiravir, and paxlovid have been approved for use in hospitalized COVID-19 patients, and additional drugs are needed. In this study, we established two cellular models relevant to COVID-19 disease that are scalable and amenable to high-throughput screening. We used this system to screen drugs that advanced to clinical trials based on *in vitro* activity against SARS-CoV-2. We noted poor antiviral activity of remdesivir in Vero cells compared with stem cell-derived lung AT2 cells and cardiac cells. These data are consistent with a previous report showing that remdesivir is metabolized inefficiently in Vero cells (Pruijssers et al., 2020) and suggests that Vero cells are not optimal for screening antiviral compounds against SARS-CoV-2.

Based on results from phosphoproteomics analysis, we screened several kinase inhibitors for their ability to inhibit viral replication in lung AT2 and cardiac cells. Out of 12 compounds we evaluated, three had activity in both AT2 and cardiac cells (SPHINX31, alectinib, abemaciclib), one had activity in AT2 cells only (SNS-032), four had activity in cardiac cells only (CCT241533, palbociclib, trilaciclib, bisindolylmaleimide I), and the remaining were ineffective. We observed that several CDK inhibitors were toxic at the concentrations tested, particularly in cardiac cells. Of note SNS-032 showed strong antiviral activity in AT2 cells but induced cardiac cell death; medicinal chemistry approaches could be explored to limit the toxicity for cardiac cells. Effectiveness of SRPK1 and CDK inhibitors against SARS-CoV-2 has been reported previously in Vero, Calu-3, and A549-ACE2 cells and

primary lung cells (Bouhaddou et al., 2020; Yaron et al., 2020). However, this is the first study to show potential toxicity of CDK inhibitors in cardiac cells. Although we observed antiviral activity in both cell types, SRPK1 inhibitors were effective at lower concentrations in AT2 compared with cardiac cells. Overall, we have identified several antiviral compounds with distinct effectiveness and toxicity profiles in lung AT2 and cardiac cells, highlighting the importance of using several cell types for evaluation of antiviral effectiveness.

In summary, with paired experiments in human stem cell-derived tissue surrogates of organs that are affected in severe COVID-19, we have demonstrated important commonalities and several key differences in virus-host interactions in lung and cardiac cells. While the value of using human lung organoids and A549 and Calu-3 cells for evaluation of antiviral drugs has been recognized, our work highlights the importance of evaluation in additional relevant cells (lung and heart) for the evaluation of antiviral activity and cytotoxicity of drugs that are considered for treatment of COVID-19. This parallel evaluation in two cell types offers novel insights into the rational design of therapeutic interventions.

EXPERIMENTAL PROCEDURES

Resource availability

Corresponding authors

Enzo R. Porrello, Jose M. Polo, Sean J. Humphrey, Mirana Ramialison, David A. Elliott or Kanta Subbarao are the corresponding authors for this paper.

Materials availability

All stem cells and immortalized cell lines are available upon request from D.A.E. and K.S. ACE2 KO H9 and MCRIi010-A cells are available upon request from D.A.E. All plasmids for ACE2 antibodies are available upon request from W.-H.T.

Data availability

Enzo R. Porrello (cardiac), Jose M. Polo (lung), Sean J. Humphrey (proteomics), Mirana Ramialison (transcriptomics), David A. Elliott (hESC- and hiPSC lines; cardiac) and Kanta Subbarao (SARS-CoV-2). The accession number for the RNA-Seq data reported in this paper is NCBI GEO: GSE212003. The accession number for the raw and Spectronaut-processed phosphoproteomics data reported in this paper is PRIDE:PXD037615.

Cells

African green monkey kidney epithelial (Vero cells, ATCC Cat. CCL-81), Vero hSLAM (Merck, Cat. 04091501), Calu-3 (ATCC, Cat. HTB-55), and VeroE6-TMPRSS2 (CellBank Australia, Cat. JCRB1819) cells were cultured at 37°C and 5% CO_2. Vero cell media: minimum essential medium (MEM; Media Preparation Unit, Peter Doherty Institute) supplemented with 5% fetal bovine serum (FBS; Bovogen, Cat. SFBS), 50 U/mL penicillin and 50 μg/mL streptomycin (PenStrep, Thermo Fisher Scientific, Cat. 15070-063), 2 mM GlutaMAX (Thermo Fisher Scientific, Cat. 35050061), and 15 mM HEPES (Thermo Fisher Scientific, Cat. 15630130). Vero hSLAM cell media: MEM supplemented with 7% FBS, PenStrep, 2 mM GlutaMAX, 15 mM HEPES, and 0.4 mg/mL G418 Sulfate (Gibco, Cat. 10131027). Calu-3 cell media: MEM containing L-glutamine and sodium bicarbonate (Sigma, Cat. M4655) supplemented with 10% FBS, PenStrep, 1× non-essential amino acids (Gibco, Cat. 11140050), and sodium pyruvate (Fisher Scientific, Cat. BP356-100). VeroE6-TMPRSS2 cell media: Dulbecco's MEM (DMEM; Media Preparation Unit, Peter Doherty Institute) supplemented with 10% FBS, PenStrep, 2 mM GlutaMAX, and 1 mg/mL G418 Sulfate.

Viruses

SARS-CoV-2 viruses hCoV-19/Australia/VIC01/2020 (VIC01, GISAID: EPI_ISL_406844), hCoV-19/Australia/VIC17991/2020 (Alpha variant, GISAID: EPI_ISL_779606), hCoV-19/Australia/QLD1520/2020 (Beta variant, GISAID: EPI_ISL_968081), hCoV-19/Australia/VIC18440/2021 (Delta variant, GISAID: EPI_ISL_1913206), hCoV-19/Australia/NSW-RPAH-1933/2021 (Omicron BA.1 variant, GISAID: EPI_ISL_6814922), and hCoV-19/Australia/VIC35864/2022 (Omicron BA.2 variant, GISAID: EPI_ISL_8955536) were kind gifts from the Victorian Infectious Diseases Reference Laboratory (VIDRL). hCoV-19/Japan/TY7-503/2021 (Gamma variant, GISAID: EPI_ISL_877769, NR-54982) was obtained through BEI Resources, NIAID, NIH, contributed by the National Institute of Infectious Diseases. The icSARS-CoV-2-nLuc virus was a kind gift from Prof. Ralph S. Baric from the Department of Microbiology and Immunology, University of North Carolina at Chapel Hill, Chapel Hill, NC, USA (Hou et al., 2020). SARS-CoV-2 VIC01 was propagated in Vero and Vero hSLAM cells in Vero infection medium (serum-free MEM in the presence of 1 μg/mL TPCK-Trypsin [Cat. LS003740]). SARS-CoV-2 Alpha, Beta, Gamma, and Delta variants were propagated in Vero hSLAM cells in infection medium (serum-free MEM with 1 μg/mL TPCK-trypsin). SARS-CoV-2 Omicron BA.1 and BA.2 variants were passaged in Calu3 cells in infection media (MEM containing 2% FBS). Virus stocks were stored at −80°C and titered as described below.

Virus titration

Virus titrations were performed in 96-well plates with confluent Vero and VeroE6-TMPRSS2 monolayers. Cells were washed with plain MEM and replaced with 180 μL serum-free media containing 1 μg/mL TPCK-trypsin. Each sample was titrated in quadruplicate by adding 20 μL supernatant to the first well and performing 10-fold serial dilutions. Cells were incubated at 37°C and assessed microscopically for SARS-CoV-2-induced cytopathic effect (CPE) on day 4. Virus titers are expressed as mean $\log_{10}TCID_{50}$/mL.

Viral RNA extraction and RT-PCR

RNA was extracted as per the manufacturer's recommendation using QiaCube HT (Qiagen) and QiaAmp 96 Virus QiaCube HT kit (Qiagen, Cat. 57731). RT-PCR reaction was set up using SensiFast Probe No-ROX One-Step Kit (Bioline, Cat. BIO-76005) using the following primers/probes: E_Sarbeco_F1: 5′-ACAGGTACGTTAA TAGTTAATAGCGT-3′, E_Sarbeco_R2: 5′-ATATTGCAGCAGTACG CACACA-3′), and E_Sarbeco_P1_FAM: 5′-ACACTAGCCATCCT

TACTGCGCTTCG-3′. Serial 10-fold dilutions of plasmid encoding the viral E gene were used to generate a standard curve for calculating the virus genome copies in the samples.

Lung AT2 cell differentiation

H9 embryonic (female) stem cells were seeded onto flasks coated with Matrigel (Corning, Cat. 354230) in Essential 8 medium (Thermo Fisher Scientific, Cat. A1517001). After 48 h, medium was changed daily with RPMI 1640 (Thermo Fisher Scientific, Cat. 21870084) supplemented with B-27 (Gibco, Cat. 17504044), 100 ng/mL activin A (Peprotech, Cat. 120-14P), 1 μM CHIR99021 (Sigma-Aldrich, Cat. SML1046), and PenStrep for 3 days. On days 4–8, the medium was changed daily with DMEM/F12 media (Thermo Fisher Scientific, Cat. 105650) supplemented with N2 (Gibco, Cat. 17502048), B27, 0.05 mg/mL ascorbic acid (Sigma-Aldrich, Cat. A92902), 0.4 mM monothioglycerol (Sigma-Aldrich, Cat. M6145), 2 μM dorsomorphin (Stemcell Technologies, Cat. 72102), SB431542 (Miltenyi Biotec, Cat. 130-106-543), and PenStrep. On days 9–12, the medium was changed daily with DMEM/F12-based medium with B27, 0.05 mg/mL ascorbic acid, 0.4 mM monothioglycerol, 20 ng/mL BMP4 (Peprotech, Cat. 120-05ET), 0.5 μM retinoic acid (ATRA; Sigma-Aldrich, Cat. R2625), 3 μM CHIR99021, and PenStrep. From day 12 onward, the medium was changed every other day with DMEM/F12 supplemented with B27, 0.05 mg/mL ascorbic acid, 0.4 mM monothioglycerol, 10 ng/mL FGF10 (Stemcell Technologies, Cat. 78037), 10 ng/mL FGF7 (Peprotech, Cat. 10019), 3 μM CHIR99021, 50 nM dexamethasone (Sigma-Aldrich, Cat. D4902), 0.1 mM 8-bromoadenosine 3′,5′-cyclic monophosphate (8-Br-cAMP; Sigma-Aldrich, Cat. B5386), 0.1 mM 3-isobutyl-1-methylxanthine (IBMX; Sigma-Aldrich, Cat. I5879), and PenStrep. Cultures were embedded onto Matrigel on day 18 in 12-well plates. On day 30, organoids were dissociated in TrypLE (Thermo Fisher Scientific, Cat. 12604013) for 3 min before being re-embedded in Matrigel. Lung organoids were maintained for experiments between passages 2 and 8 prior to dissociation with TrypLE and seeding onto Geltrex (Gibco, Cat. A1413201)-coated plates supplemented with Y-27632 (Selleck Chemicals, Cat. S1049) at the initial seeding step. Cells were maintained for a further 7–10 days in 2D culture until infection at 70%+ confluency.

Cardiac cell differentiation

The hESC lines HES3 *NKX2-5*$^{eGFP/w}$ and H9 (both female) and the hiPSC line MCRIi010-A (male) were used for viral infection studies in 2D monolayer cultures. Each stem cell line and their derivatives were cultured as outlined previously (Elliott et al., 2011). Cardiomyocyte cultures were differentiated as previously described and cryopreserved at day 10 following differentiation (Anderson et al., 2018). Cells were subsequently thawed in basal differentiation media containing RPMI 1640 (Thermo Fisher Scientific, Cat. 21870), 2% B27 without vitamin A (Thermo Fisher Scientific, Cat. 12587), 1% GlutaMAX (Thermo Fisher Scientific, Cat. 35050), 0.5% PenStrep (Thermo Fisher Scientific, Cat. 15070), and 10 μM Y-27632 for 24 h at 37°C. Cells were then maintained in basal differentiation medium for an additional 2 days. To enrich for cardiomyocytes, cells were cultured for 2 days in lactate purification media as described previously (Tohyama et al., 2013). The cells were maintained in maturation media, as described previously (Mills et al., 2017), from day 15 to 23 post-differentiation prior to viral infection.

Virus growth in lung AT2, cardiac, and Vero cells

Infection of hESC- and iPSC-derived cells and Vero cells was performed in 24 well tissue culture plates. Vero cells were washed with MEM prior to infection. Media were removed and replaced with 10^4 $TCID_{50}$ of SARS-CoV-2 (approx. MOI 0.1) in 100 μL and incubated for 1 h at room temperature. The inoculum was removed and cells were washed twice with cell-specific media and then refed with media. The second wash was harvested for day 0 sampling. Vero cells were cultured in serum-free media containing 1 μg/mL TPCK-trypsin. Supernatants were collected each day, and media were replenished. Harvested supernatants were stored at −80°C to determine infectious virus titers and E gene copies.

SARS-CoV-2 entry inhibition

Lung AT2 and cardiac cells seeded into 24-well plates were treated with 100 μL α-ACE2 antibodies (WCSL141 and WCSL148; Chen et al., 2021a), human immunoglobulin G (IgG) isotype control, camostat mesylate (Sigma Aldrich, Cat. SML0057), or DMSO for 1 h at 37°C. Subsequently, 10^4 $TCID_{50}$ SARS-CoV-2 was added to cells and incubated for 1 h at 37°C. Virus inoculum was removed, and cells were washed with plain MEM twice before replacement with the 500 μL cell-specific culture media. For CA-074 Me inhibition, cells seeded into 24-well plates were treated with 200 μL CA-074 Me (Selleck Chemicals, Cat. S7420) for 2 h at 37°C. Subsequently, 10^4 $TCID_{50}$ SARS-CoV-2 was added to cells and incubated for 1 h at 37°C. Supernatant samples were obtained daily, and the media was replaced with drug-containing media until day 3. Infectious virus titers and E gene copies were determined as detailed above.

Antiviral testing

Compounds remdesivir (MedChemExpress, Cat. HY104077), NHC (β-D-N4-hydroxycytidine, MedChemExpress, Cat. HY125033), favipiravir (Toyama Chemicals, Japan, T705), tizoxanide (Romark Laboratories, Tampa, FL, USA), chloroquine (Sigma Aldrich, Cat. C6628), and piperaquine (Sigma Aldrich, Cat. C7874) were tested in lung AT2, cardiac, and Vero cells in 24-well tissue culture plates. Vero cells were washed with MEM prior to the addition of 100 μL cell-type-specific media containing diluted compounds. The vehicle controls were prepared to contain the same amount of vehicle (DMSO or water) as the 10 μM compound. One hour after addition of diluted compound, 100 μL media containing 10^4 $TCID_{50}$ SARS-CoV-2 (and 1 μg/mL TPCK-trypsin for Vero cells) was added and incubated for an additional hour at room temperature. The inoculum was removed and replaced with 500 μL cell-specific media containing diluted compounds. At 3 dpi, supernatants were harvested and stored at −80°C. Infectious virus titers and E gene copies were determined as detailed above.

Kinase inhibitor compounds (Table S2) were tested in lung AT2 and cardiac cells seeded in 96-well culture plates. Cells were incubated with 200 μL cell-specific media containing 30–0.04 μM compound for 2 h at 37°C. DMSO was maintained consistently to a final concentration of 0.1%. After 2 h, 10^4 $TCID_{50}$ icSARS-CoV-2-nLuc or VIC01 (approx. MOI 1) was added to each well (20 μL total), and

cells were incubated at 37°C for 2 days. Cell supernatant from VIC01-infected cells was collected for measurement of E gene copies as detailed above. For nLuc virus detection, cells were lysed with Passive Lysis Buffer (Promega, Cat. E1941) and luciferase expression measured using Nano-Glo Luciferase Assay System (Promega, Cat. N1130) as per the manufacturer's instructions. Luminescence was measured on FLUOstar Omega (BMG Labtech).

Antiviral toxicity testing

All compounds were tested in lung AT2, cardiac, and Vero cells in 96-well tissue culture plates. Vero cells were washed with 200 μL MEM. After removal of media, 100 μL cell-type-specific media containing diluted compound was added. At day 2 (kinase inhibitors) or day 3 (other compounds), cell viability was measuring using the CellTiter-Glo2.0 cell viability kit (Promega, Cat. G9241) as per the manufacturer's recommendations. Luminescence was measured on FLUOstar Omega (BMG Labtech).

RNA-seq analysis

Human stem cell-derived cardiac and lung cells grown in 24-well tissue culture plates were infected with 10^4 $TCID_{50}$ SARS-CoV-2. At 0, 1, and 3 days post-infection, supernatant was removed, and the cell monolayer was lysed with 500 μL TRIzol reagent (Life Technologies Australia, Cat. 15596018). RNA was extracted following the manufacturer's protocol.

RNA-seq data were demultiplexed using a modified version of the Sabre demultiplexer to produce a single fastq file per sample. Fastq files were processed using the RNAsik pipeline (https://doi.org/10.21105/joss.00583). Reads were aligned to EnsEMBL GRCh38 (Howe et al., 2021) using the STAR aligner (Dobin et al., 2013), and duplicates were marked with Picard (http://broadinstitute.github.io/picard/). Aligned reads were quantified to gene level counts using featureCounts (Liao et al., 2014). Next, differential gene expression analysis was performed in Degust (https://doi.org/10.5281/zenodo.3501067) using the EdgeR QL method (Robinson et al., 2010) to produce sets of DEGs for cardiac and lung conditions, respectively. The sets of DEGs were processed for pathway enrichment using Metascape (Zhou et al., 2019) with default parameters except that only the WikiPathways ontology was used. Figures were generated using R (v.4) and tidyverse (https://doi.org/10.21105/joss.01686) packages.

LEGENDplex

Cytokine/chemokine concentrations in supernatant from mock and SARS-CoV-2-infected lung AT2 and cardiac cells were analyzed using the LEGENDplex human antivirus response panel (BioLegend, Cat. 740390) following the manufacturer's instructions. Samples were run on a BD FACSCanto II and analyzed using LEGENDplex Data Analysis Software Suite (v.8).

Statistical analysis

All data were plotted and analyzed using GraphPad Prism 9. Log_{10} virus titers and E gene copies were analyzed using either a Student's t test or two-way ANOVA with Tukey's or Dunnett's multiple comparisons test as appropriate. *$p < 0.05$, **$p < 0.01$, ***$p < 0.001$, and ****$p < 0.0001$. Dotted lines indicate the lower limit of detection of the assay unless indicated otherwise. Data are representative of at least two independent experiments showing mean (±SD) unless indicated overwise. Antiviral activity and cytotoxicity data for the kinase inhibitors (Figures 5 and S7) were analyzed by calculating the percentage of inhibition/viability relative to vehicle control. Curve fitting was performed using non-linear regression (four parameters – variable slope) with data constrained between 0 and 100.

ETHICS APPROVAL

No animals were used in this study. All work at MCRI involving hESCs and hiPSCs was approved by The Royal Children's Hospital Human Research Ethics Committee (HREC 33001 A) and all work at Monash University involving hESCs was approved under Human Ethics Application ERM# 23170.

SUPPLEMENTAL INFORMATION

Supplemental information can be found online at https://doi.org/10.1016/j.stemcr.2023.05.007.

AUTHOR CONTRIBUTIONS

Conceptualization and design, E.P., J.M.P, S.J.H., M.R., D.A.E., and K.S.; data acquisition, R.R., M.J.G., J.A.N., E.S.S., J.C., E.J.D., M.S., C.M.-K., L.Y.Y.L., M.W., H.P., K.K., D.A.-B., Y.B.Y.S., and J.P.T.; data analysis and interpretation, R.R., M.J.G., J.A.N., E.S.S., J.C., E.J.D., M.S., A.S., N.C., H.T.N., and P.D.C.; reagent production, D.D. and W.-H.T.; manuscript preparation, R.R., M.J.G., J.A.N., D.A.E., and K.S.; manuscript edits and proofing, E.S.S., J.C., E.J.D., M.S., E.P., J.M.P., S.J.H., and M.R. All authors critically reviewed and approved the final version of the manuscript.

ACKNOWLEDGMENTS

This work was supported by The Medical Research Future Fund (MRF9200007; K.S., E.P., J.M.P., D.A.E.), the Victorian State Government (Victorian State Government (DJPR/COVID-19; K.S., M.R., E.P., J.M.P., D.A.E.), and the COVID-19 Victorian Consortium (K.S.). E.P., M.R., and D.A.E. are supported by The Novo Nordisk Foundation Center for Stem Cell Medicine (grant NNF21CC0073729), The Stafford Fox Medical Research Foundation, and The Royal Children's Hospital Foundation. Fellowship support was provided by the National Health and Medical Research Council of Australia (E.P. and K.S.). MCRI is supported by the Victorian Government's Operational Infrastructure Support Program. The Melbourne WHO Collaborating Center for Reference and Research on Influenza is supported by the Australian Government Department of Health.

CONFLICT OF INTERESTS

E.P. is a co-founder and scientific advisor and holds equity in, and N.C. has a paid position with, Dynomics, a biotechnology company focused on the development of heart failure therapeutics. J.M.P. is a co-founder and shareholder of Mogrify, Ltd., a cell therapy company.

Received: March 23, 2023
Revised: May 10, 2023
Accepted: May 11, 2023
Published: June 13, 2023

REFERENCES

Anderson, D.J., Kaplan, D.I., Bell, K.M., Koutsis, K., Haynes, J.M., Mills, R.J., Phelan, D.G., Qian, E.L., Leitoguinho, A.R., Arasaratnam, D., et al. (2018). NKX2-5 regulates human cardiomyogenesis via a HEY2 dependent transcriptional network. Nat. Commun. *9*, 1373. https://doi.org/10.1038/s41467-018-03714-x.

Bailey, A.L., Dmytrenko, O., Greenberg, L., Bredemeyer, A.L., Ma, P., Liu, J., Penna, V., Winkler, E.S., Sviben, S., Brooks, E., et al. (2021). SARS-CoV-2 infects human engineered heart tissues and models COVID-19 myocarditis. JACC Basic Transl Sci *6*, 331–345. https://doi.org/10.1016/j.jacbts.2021.01.002.

Bojkova, D., Wagner, J.U.G., Shumliakivska, M., Aslan, G.S., Saleem, U., Hansen, A., Luxán, G., Günther, S., Pham, M.D., Krishnan, J., et al. (2020). SARS-CoV-2 infects and induces cytotoxic effects in human cardiomyocytes. Cardiovasc. Res. *116*, 2207–2215. https://doi.org/10.1093/cvr/cvaa267.

Bouhaddou, M., Memon, D., Meyer, B., White, K.M., Rezelj, V.V., Correa Marrero, M., Polacco, B.J., Melnyk, J.E., Ulferts, S., Kaake, R.M., et al. (2020). The global phosphorylation landscape of SARS-CoV-2 infection. Cell *182*, 685–712.e19. https://doi.org/10.1016/j.cell.2020.06.034.

Chen, J., Gao, K., Wang, R., and Wei, G.W. (2021a). An iTSC-derived placental model of SARS-CoV-2 infection reveals ACE2-dependent susceptibility in syncytiotrophoblasts. bioRxiv. https://doi.org/10.1101/2021.10.27.465224.

Chen, P.Z., Bobrovitz, N., Premji, Z.A., Koopmans, M., Fisman, D.N., and Gu, F.X. (2021b). SARS-CoV-2 shedding dynamics across the respiratory tract, sex, and disease severity for adult and pediatric COVID-19. Elife *10*, e70458. https://doi.org/10.7554/eLife.70458.

Deinhardt-Emmer, S., Wittschieber, D., Sanft, J., Kleemann, S., Elschner, S., Haupt, K.F., Vau, V., Häring, C., Rödel, J., Henke, A., et al. (2021). Early postmortem mapping of SARS-CoV-2 RNA in patients with COVID-19 and the correlation with tissue damage. Elife *10*, e60361. https://doi.org/10.7554/eLife.60361.

Dobin, A., Davis, C.A., Schlesinger, F., Drenkow, J., Zaleski, C., Jha, S., Batut, P., Chaisson, M., and Gingeras, T.R. (2013). STAR: ultrafast universal RNA-seq aligner. Bioinformatics *29*, 15–21. https://doi.org/10.1093/bioinformatics/bts635.

Elliott, D.A., Braam, S.R., Koutsis, K., Ng, E.S., Jenny, R., Lagerqvist, E.L., Biben, C., Hatzistavrou, T., Hirst, C.E., Yu, Q.C., et al. (2011). NKX2-5(eGFP/w) hESCs for isolation of human cardiac progenitors and cardiomyocytes. Nat. Methods *8*, 1037–1040. https://doi.org/10.1038/nmeth.1740.

Goyal, P., Choi, J.J., Pinheiro, L.C., Schenck, E.J., Chen, R., Jabri, A., Satlin, M.J., Campion, T.R., Jr., Nahid, M., Ringel, J.B., et al. (2020). Clinical characteristics of Covid-19 in New York City. N. Engl. J. Med. *382*, 2372–2374. https://doi.org/10.1056/NEJMc2010419.

Gunst, J.D., Staerke, N.B., Pahus, M.H., Kristensen, L.H., Bodilsen, J., Lohse, N., Dalgaard, L.S., Brønnum, D., Fröbert, O., Hønge, B., et al. (2021). Efficacy of the TMPRSS2 inhibitor camostat mesilate in patients hospitalized with Covid-19-a double-blind randomized controlled trial. EClinicalMedicine *35*, 100849. https://doi.org/10.1016/j.eclinm.2021.100849.

Hamming, I., Timens, W., Bulthuis, M.L.C., Lely, A.T., Navis, G.J., and van Goor, H. (2004). Tissue distribution of ACE2 protein, the functional receptor for SARS coronavirus. A first step in understanding SARS pathogenesis. J. Pathol. *203*, 631–637. https://doi.org/10.1002/path.1570.

Hoffmann, M., Kleine-Weber, H., Schroeder, S., Krüger, N., Herrler, T., Erichsen, S., Schiergens, T.S., Herrler, G., Wu, N.H., Nitsche, A., et al. (2020). SARS-CoV-2 cell entry depends on ACE2 and TMPRSS2 and is blocked by a clinically proven protease inhibitor. Cell *181*, 271–280.e8. https://doi.org/10.1016/j.cell.2020.02.052.

Hou, Y.J., Okuda, K., Edwards, C.E., Martinez, D.R., Asakura, T., Dinnon, K.H., 3rd, Kato, T., Lee, R.E., Yount, B.L., Mascenik, T.M., et al. (2020). SARS-CoV-2 reverse genetics reveals a variable infection gradient in the respiratory tract. Cell *182*, 429–446.e14. https://doi.org/10.1016/j.cell.2020.05.042.

Howe, K.L., Achuthan, P., Allen, J., Allen, J., Alvarez-Jarreta, J., Amode, M.R., Armean, I.M., Azov, A.G., Bennett, R., Bhai, J., et al. (2021). Ensembl 2021. Nucleic Acids Res. *49*, D884–D891. https://doi.org/10.1093/nar/gkaa942.

Huang, J., Hume, A.J., Abo, K.M., Werder, R.B., Villacorta-Martin, C., Alysandratos, K.D., Beermann, M.L., Simone-Roach, C., Lindstrom-Vautrin, J., Olejnik, J., et al. (2020). SARS-CoV-2 infection of pluripotent stem cell-derived human lung alveolar type 2 cells elicits a rapid epithelial-intrinsic inflammatory response. Cell Stem Cell *27*, 962–973.e7. https://doi.org/10.1016/j.stem.2020.09.013.

Humphrey, S.J., Karayel, O., James, D.E., and Mann, M. (2018). High-throughput and high-sensitivity phosphoproteomics with the EasyPhos platform. Nat. Protoc. *13*, 1897–1916. https://doi.org/10.1038/s41596-018-0014-9.

Jacob, A., Morley, M., Hawkins, F., McCauley, K.B., Jean, J.C., Heins, H., Na, C.L., Weaver, T.E., Vedaie, M., Hurley, K., et al. (2017). Differentiation of human pluripotent stem cells into functional lung alveolar epithelial cells. Cell Stem Cell *21*, 472–488.e10. https://doi.org/10.1016/j.stem.2017.08.014.

Katsura, H., Sontake, V., Tata, A., Kobayashi, Y., Edwards, C.E., Heaton, B.E., Konkimalla, A., Asakura, T., Mikami, Y., Fritch, E.J., et al. (2020). Human lung stem cell-based alveolospheres provide insights into SARS-CoV-2-mediated interferon responses and pneumocyte dysfunction. Cell Stem Cell *27*, 890–904.e8. https://doi.org/10.1016/j.stem.2020.10.005.

Lazzerini, P.E., Laghi-Pasini, F., Boutjdir, M., and Capecchi, P.L. (2022). Inflammatory cytokines and cardiac arrhythmias: the lesson from COVID-19. Nat. Rev. Immunol. *22*, 270–272. https://doi.org/10.1038/s41577-022-00714-3.

Lee, C.Y., Huang, C.H., Rastegari, E., Rengganaten, V., Liu, P.C., Tsai, P.H., Chin, Y.F., Wu, J.R., Chiou, S.H., Teng, Y.C., et al. (2021). Tumor necrosis factor-alpha exacerbates viral entry in SARS-CoV2-infected iPSC-derived cardiomyocytes. Int. J. Mol. Sci. *22*, 9869. https://doi.org/10.3390/ijms22189869.

Lei, X., Dong, X., Ma, R., Wang, W., Xiao, X., Tian, Z., Wang, C., Wang, Y., Li, L., Ren, L., et al. (2020). Activation and evasion of type I interferon responses by SARS-CoV-2. Nat. Commun. *11*, 3810. https://doi.org/10.1038/s41467-020-17665-9.

Li, Y., Renner, D.M., Comar, C.E., Whelan, J.N., Reyes, H.M., Cardenas-Diaz, F.L., Truitt, R., Tan, L.H., Dong, B., Alysandratos, K.D., et al. (2021). SARS-CoV-2 induces double-stranded RNA-mediated innate immune responses in respiratory epithelial-derived cells and cardiomyocytes. Proc. Natl. Acad. Sci. USA *118*. e2022643118. https://doi.org/10.1073/pnas.2022643118.

Liao, Y., Smyth, G.K., and Shi, W. (2014). featureCounts: an efficient general purpose program for assigning sequence reads to genomic features. Bioinformatics *30*, 923–930. https://doi.org/10.1093/bioinformatics/btt656.

Lopes, L.R., Garcia-Hernández, S., Lorenzini, M., Futema, M., Chumakova, O., Zateyshchikov, D., Isidoro-Garcia, M., Villacorta, E., Escobar-Lopez, L., Garcia-Pavia, P., et al. (2021). Alpha-protein kinase 3 (ALPK3) truncating variants are a cause of autosomal dominant hypertrophic cardiomyopathy. Eur. Heart J. *42*, 3063–3073. https://doi.org/10.1093/eurheartj/ehab424.

Marchiano, S., Hsiang, T.Y., Khanna, A., Higashi, T., Whitmore, L.S., Bargehr, J., Davaapil, H., Chang, J., Smith, E., Ong, L.P., et al. (2021). SARS-CoV-2 infects human pluripotent stem cell-derived cardiomyocytes, impairing electrical and mechanical function. Stem Cell Rep. *16*, 478–492. https://doi.org/10.1016/j.stemcr.2021.02.008.

Mills, R.J., Titmarsh, D.M., Koenig, X., Parker, B.L., Ryall, J.G., Quaife-Ryan, G.A., Voges, H.K., Hodson, M.P., Ferguson, C., Drowley, L., et al. (2017). Functional screening in human cardiac organoids reveals a metabolic mechanism for cardiomyocyte cell cycle arrest. Proc. Natl. Acad. Sci. USA *114*, E8372–E8381. https://doi.org/10.1073/pnas.1707316114.

Montaser, M., Lalmanach, G., and Mach, L. (2002). CA-074, but not its methyl ester CA-074Me, is a selective inhibitor of cathepsin B within living cells. Biol. Chem. *383*, 1305–1308. https://doi.org/10.1515/BC.2002.147.

Mulay, A., Konda, B., Garcia, G., Jr., Yao, C., Beil, S., Villalba, J.M., Koziol, C., Sen, C., Purkayastha, A., Kolls, J.K., et al. (2021). SARS-CoV-2 infection of primary human lung epithelium for COVID-19 modeling and drug discovery. Cell Rep. *35*, 109055. https://doi.org/10.1016/j.celrep.2021.109055.

Muus, C., Luecken, M.D., Eraslan, G., Sikkema, L., Waghray, A., Heimberg, G., Kobayashi, Y., Vaishnav, E.D., Subramanian, A., Smillie, C., et al. (2021). Single-cell meta-analysis of SARS-CoV-2 entry genes across tissues and demographics. Nat. Med. *27*, 546–559. https://doi.org/10.1038/s41591-020-01227-z.

Nalbandian, A., Sehgal, K., Gupta, A., Madhavan, M.V., McGroder, C., Stevens, J.S., Cook, J.R., Nordvig, A.S., Shalev, D., Sehrawat, T.S., et al. (2021). Post-acute COVID-19 syndrome. Nat. Med. *27*, 601–615. https://doi.org/10.1038/s41591-021-01283-z.

Navaratnarajah, C.K., Pease, D.R., Halfmann, P.J., Taye, B., Barkhymer, A., Howell, K.G., Charlesworth, J.E., Christensen, T.A., Kawaoka, Y., Cattaneo, R., et al. (2021). Highly efficient SARS-CoV-2 infection of human cardiomyocytes: spike protein-mediated cell fusion and its inhibition. J. Virol. *95*, e0136821. https://doi.org/10.1128/JVI.01368-21.

Ou, X., Liu, Y., Lei, X., Li, P., Mi, D., Ren, L., Guo, L., Guo, R., Chen, T., Hu, J., et al. (2020). Characterization of spike glycoprotein of SARS-CoV-2 on virus entry and its immune cross-reactivity with SARS-CoV. Nat. Commun. *11*, 1620. https://doi.org/10.1038/s41467-020-15562-9.

Perez-Bermejo, J.A., Kang, S., Rockwood, S.J., Simoneau, C.R., Joy, D.A., Silva, A.C., Ramadoss, G.N., Flanigan, W.R., Fozouni, P., Li, H., et al. (2021). SARS-CoV-2 infection of human iPSC-derived cardiac cells reflects cytopathic features in hearts of patients with COVID-19. Sci. Transl. Med. *13*, eabf7872. https://doi.org/10.1126/scitranslmed.abf7872.

Phelan, D.G., Anderson, D.J., Howden, S.E., Wong, R.C.B., Hickey, P.F., Pope, K., Wilson, G.R., Pébay, A., Davis, A.M., Petrou, S., et al. (2016). ALPK3-deficient cardiomyocytes generated from patient-derived induced pluripotent stem cells and mutant human embryonic stem cells display abnormal calcium handling and establish that ALPK3 deficiency underlies familial cardiomyopathy. Eur. Heart J. *37*, 2586–2590. https://doi.org/10.1093/eurheartj/ehw160.

Pruijssers, A.J., George, A.S., Schäfer, A., Leist, S.R., Gralinksi, L.E., Dinnon, K.H., 3rd, Yount, B.L., Agostini, M.L., Stevens, L.J., Chappell, J.D., et al. (2020). Remdesivir inhibits SARS-CoV-2 in human lung cells and chimeric SARS-CoV expressing the SARS-CoV-2 RNA polymerase in mice. Cell Rep. *32*, 107940. https://doi.org/10.1016/j.celrep.2020.107940.

Puntmann, V.O., Carerj, M.L., Wieters, I., Fahim, M., Arendt, C., Hoffmann, J., Shchendrygina, A., Escher, F., Vasa-Nicotera, M., Zeiher, A.M., et al. (2020). Outcomes of cardiovascular magnetic resonance imaging in patients recently recovered from coronavirus disease 2019 (COVID-19). JAMA Cardiol. *5*, 1265–1273. https://doi.org/10.1001/jamacardio.2020.3557.

Qi, F., Qian, S., Zhang, S., and Zhang, Z. (2020). Single cell RNA sequencing of 13 human tissues identify cell types and receptors of human coronaviruses. Biochem. Biophys. Res. Commun. *526*, 135–140. https://doi.org/10.1016/j.bbrc.2020.03.044.

Robinson, E.L., Alkass, K., Bergmann, O., Maguire, J.J., Roderick, H.L., and Davenport, A.P. (2020). Genes encoding ACE2, TMPRSS2 and related proteins mediating SARS-CoV-2 viral entry are upregulated with age in human cardiomyocytes. J. Mol. Cell. Cardiol. *147*, 88–91. https://doi.org/10.1016/j.yjmcc.2020.08.009.

Robinson, M.D., McCarthy, D.J., and Smyth, G.K. (2010). edgeR: a Bioconductor package for differential expression analysis of digital gene expression data. Bioinformatics *26*, 139–140. https://doi.org/10.1093/bioinformatics/btp616.

Sampaio, N.G., Chauveau, L., Hertzog, J., Bridgeman, A., Fowler, G., Moonen, J.P., Dupont, M., Russell, R.A., Noerenberg, M., and Rehwinkel, J. (2021). The RNA sensor MDA5 detects SARS-CoV-2 infection. Sci. Rep. *11*, 13638. https://doi.org/10.1038/s41598-021-92940-3.

Schneider, J., Pease, D., Navaratnarajah, C., Halfmann, P., Clemens, D., Ye, D., Kim, C., Barkhymer, A., Cohle, S., Banks, A., et al. (2020). SARS-CoV-2 direct cardiac damage through spike-mediated cardiomyocyte fusion. Research Square.

Shang, J., Wan, Y., Luo, C., Ye, G., Geng, Q., Auerbach, A., and Li, F. (2020). Cell entry mechanisms of SARS-CoV-2. Proc. Natl. Acad.

Sci. USA *117*, 11727–11734. https://doi.org/10.1073/pnas.2003138117.

Shao, M.J., Shang, L.X., Luo, J.Y., Shi, J., Zhao, Y., Li, X.M., and Yang, Y.N. (2020). Myocardial injury is associated with higher mortality in patients with coronavirus disease 2019: a meta-analysis. J. Geriatr. Cardiol. *17*, 224–228. https://doi.org/10.11909/j.issn.1671-5411.2020.04.009.

Sharma, A., Garcia, G., Jr., Wang, Y., Plummer, J.T., Morizono, K., Arumugaswami, V., and Svendsen, C.N. (2020). Human iPSC-derived cardiomyocytes are susceptible to SARS-CoV-2 infection. Cell Rep. Med. *1*, 100052. https://doi.org/10.1016/j.xcrm.2020.100052.

Shemesh, M., Aktepe, T.E., Deerain, J.M., McAuley, J.L., Audsley, M.D., David, C.T., Purcell, D.F.J., Urin, V., Hartmann, R., Moseley, G.W., et al. (2021). SARS-CoV-2 suppresses IFNbeta production mediated by NSP1, 5, 6, 15, ORF6 and ORF7b but does not suppress the effects of added interferon. PLoS Pathog. *17*, e1009800. https://doi.org/10.1371/journal.ppat.1009800.

Shi, S., Qin, M., Shen, B., Cai, Y., Liu, T., Yang, F., Gong, W., Liu, X., Liang, J., Zhao, Q., et al. (2020). Association of cardiac injury with mortality in hospitalized patients with COVID-19 in Wuhan, China. JAMA Cardiol. *5*, 802–810. https://doi.org/10.1001/jamacardio.2020.0950.

Sungnak, W., Huang, N., Bécavin, C., Berg, M., Queen, R., Litvinukova, M., Talavera-López, C., Maatz, H., Reichart, D., Sampaziotis, F., et al. (2020). SARS-CoV-2 entry factors are highly expressed in nasal epithelial cells together with innate immune genes. Nat. Med. *26*, 681–687. https://doi.org/10.1038/s41591-020-0868-6.

Tiwari, S.K., Wang, S., Smith, D., Carlin, A.F., and Rana, T.M. (2021). Revealing tissue-specific SARS-CoV-2 infection and host responses using human stem cell-derived lung and cerebral organoids. Stem Cell Rep. *16*, 437–445. https://doi.org/10.1016/j.stemcr.2021.02.005.

Tohyama, S., Hattori, F., Sano, M., Hishiki, T., Nagahata, Y., Matsuura, T., Hashimoto, H., Suzuki, T., Yamashita, H., Satoh, Y., et al. (2013). Distinct metabolic flow enables large-scale purification of mouse and human pluripotent stem cell-derived cardiomyocytes. Cell Stem Cell *12*, 127–137. https://doi.org/10.1016/j.stem.2012.09.013.

Uhlén, M., Fagerberg, L., Hallström, B.M., Lindskog, C., Oksvold, P., Mardinoglu, A., Sivertsson, Å., Kampf, C., Sjöstedt, E., Asplund, A., et al. (2015). Proteomics. Tissue-based map of the human proteome. Science *347*, 1260419. https://doi.org/10.1126/science.1260419.

Wang, X.M., Mannan, R., Xiao, L., Abdulfatah, E., Qiao, Y., Farver, C., Myers, J.L., Zelenka-Wang, S., McMurry, L., Su, F., et al. (2021). Characterization of SARS-CoV-2 and host entry factors distribution in a COVID-19 autopsy series. Commun. Med. *1*, 24. https://doi.org/10.1038/s43856-021-00025-z.

Williams, T.L., Colzani, M.T., Macrae, R.G.C., Robinson, E.L., Bloor, S., Greenwood, E.J.D., Zhan, J.R., Strachan, G., Kuc, R.E., Nyimanu, D., et al. (2021). Human embryonic stem cell-derived cardiomyocyte platform screens inhibitors of SARS-CoV-2 infection. Commun. Biol. *4*, 926. https://doi.org/10.1038/s42003-021-02453-y.

Xia, H., Cao, Z., Xie, X., Zhang, X., Chen, J.Y.C., Wang, H., Menachery, V.D., Rajsbaum, R., and Shi, P.Y. (2020). Evasion of type I interferon by SARS-CoV-2. Cell Rep. *33*, 108234. https://doi.org/10.1016/j.celrep.2020.108234.

Yang, J., Chen, T., and Zhou, Y. (2021). Mediators of SARS-CoV-2 entry are preferentially enriched in cardiomyocytes. Hereditas *158*, 4. https://doi.org/10.1186/s41065-020-00168-4.

Yaron, T.M., Heaton, B.E., Levy, T.M., Johnson, J.L., Jordan, T.X., Cohen, B.M., Kerelsky, A., Lin, T.Y., Liberatore, K.M., Bulaon, D.K., et al. (2020). The FDA-approved drug Alectinib compromises SARS-CoV-2 nucleocapsid phosphorylation and inhibits viral infection in vitro. bioRxiv. https://doi.org/10.1101/2020.08.14.251207.

Youk, J., Kim, T., Evans, K.V., Jeong, Y.I., Hur, Y., Hong, S.P., Kim, J.H., Yi, K., Kim, S.Y., Na, K.J., et al. (2020). Three-dimensional human alveolar stem cell culture models reveal infection response to SARS-CoV-2. Cell Stem Cell *27*, 905–919.e10. https://doi.org/10.1016/j.stem.2020.10.004.

Zhang, Q., Bastard, P., Liu, Z., Le Pen, J., Moncada-Velez, M., Chen, J., Ogishi, M., Sabli, I.K.D., Hodeib, S., Korol, C., et al. (2020). Inborn errors of type I IFN immunity in patients with life-threatening COVID-19. Science *370*, eabd4570. https://doi.org/10.1126/science.abd4570.

Zhou, P., Yang, X.L., Wang, X.G., Hu, B., Zhang, L., Zhang, W., Si, H.R., Zhu, Y., Li, B., Huang, C.L., et al. (2020). Addendum: a pneumonia outbreak associated with a new coronavirus of probable bat origin. Nature *588*, E6. https://doi.org/10.1038/s41586-020-2951-z.

Zhou, Y., Zhou, B., Pache, L., Chang, M., Khodabakhshi, A.H., Tanaseichuk, O., Benner, C., and Chanda, S.K. (2019). Metascape provides a biologist-oriented resource for the analysis of systems-level datasets. Nat. Commun. *10*, 1523. https://doi.org/10.1038/s41467-019-09234-6.

Zou, X., Chen, K., Zou, J., Han, P., Hao, J., and Han, Z. (2020). Single-cell RNA-seq data analysis on the receptor ACE2 expression reveals the potential risk of different human organs vulnerable to 2019-nCoV infection. Front. Med. *14*, 185–192. https://doi.org/10.1007/s11684-020-0754-0.